

# Database-driven high-throughput study for hybrid perovskite coating materials

Azimatu Seidu, Lauri Himanen, Jingrui Li, and Patrick Rinke

Department of Applied Physics, Aalto University, P.O.Box 11100, FI-00076 AALTO, Finland

We developed a high-throughput screening scheme to acquire candidate coating materials for hybrid perovskites. From more than 1.8 million entries of an inorganic compound database, we collected 93 binary and ternary materials with promising properties for protectively coating halide-perovskite photoabsorbers in perovskite solar cells. These candidates fulfill a series of criteria, including wide band gaps, abundant and non-toxic elements, water-insoluble, and small lattice mismatch with surface models of halide perovskites.

Perovskite solar cells (PSCs)<sup>1-3</sup> have recently reached a power-conversion efficiency (PCE) of >23% only six years after the invention of the state-of-the-art PSC architecture in 2012 (PCE~10%)<sup>4,5</sup>. This has revived the hope for direct conversion of sustainable, affordable and environmentally friendly solar energy into electricity. The photoabsorbers in PSCs are hybrid (organic-inorganic) perovskites (denoted ABX<sub>3</sub> hereafter) especially methylammonium (MA) lead iodide (CH<sub>3</sub>NH<sub>3</sub>PbI<sub>3</sub> ≡ MAPbI<sub>3</sub>). The salient properties of these materials in optoelectronic applications are optimal band gaps, excellent absorption in the visible range of the solar spectrum, good transport properties for both electrons and holes, flexibility of composition engineering, as well as low costs in both raw materials and fabrication<sup>1,2,6-9</sup>.

Despite the excellent PSC-performance in the laboratory, stability problems limit the development and commercialization of this promising materials class. Hybrid perovskites degrade quickly in heat, oxygen and moisture<sup>10-14</sup>. With increasing exposure to any of these destabilizing factors, the structure of the hybrid perovskite degrades and the PCE reduces concomitantly after several days or even hours<sup>15,16</sup>. Among the solutions that have been proposed to solve this stability and longevity problem are protective coating<sup>17-19</sup>, the use of two-dimensional perovskites<sup>20-23</sup>, and doping with small ions<sup>14,24-27</sup>. Protective coating is particularly promising, as it can passivate the surface dangling bonds of the perovskite photoabsorber and insulate the perovskite from heat and small molecules from the environment. A good coating should have the following properties: (i) a wide band gap (>3 eV), (ii) little impact on the structure of the coated perovskite, (iii) good transport properties, and (iv) high stability in heat, air and water. It would be particularly attractive, if the coating material could also be used as a semiconducting interlayer, a key component in the modern perovskite-based device architectures. In this context, we are especially interested in cheap and efficient hole-transporting coatings, as *Spiro*-OMeTAD, the most common hole-transporting material (HTM) in PSCs since the birth of this technology<sup>4,5</sup>, is expensive, has low charge-carrier mobilities and a negative impact on PSC stability<sup>28</sup>.

We here present a database-driven high-throughput study that explores a wide range of possible candi-

dates to find inorganic materials that have the potential to protectively coat perovskites in PSCs. We take the inorganic materials from the “Automatic Flow for Materials Discovery” (AFLOW) database<sup>29</sup>. AFLOW contains nearly 2 million material entries that were computed with density-functional-theory (DFT) using the Perdew-Burke-Ernzerhof (PBE) exchange-correlation functional<sup>30</sup>.

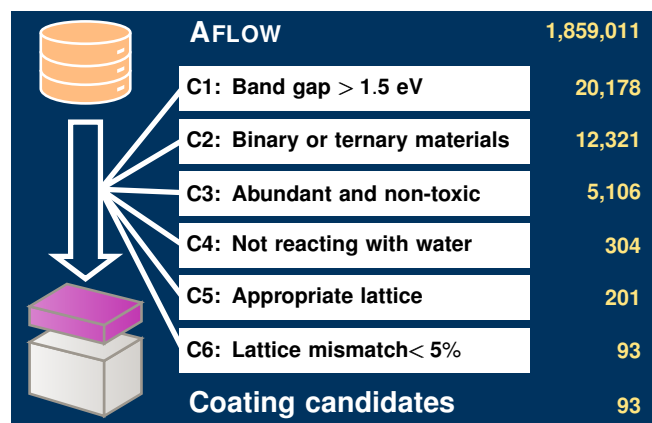


FIG. 1. High-throughput screening scheme to extract possible coating materials from AFLOW. The six filtering criteria are listed in the middle and the corresponding number of remaining compounds is given by the numbers in yellow.

In the following, we will describe our filtering scheme with which we reduced the large number of database entries to only those material candidates with promising coating properties. The workflow is illustrated in Fig. 1. Since PBE generally underestimates band gaps by ~50%<sup>31</sup>, we set our first criterion (C1) to screen materials with “PBE band gap >1.5 eV”. Considering the technical difficulties of coating with quaternary or even more complicated compounds<sup>32,33</sup>, we limited our target materials to binary and ternary compounds in this work (C2). In C3 we excluded all compounds that contain toxic or rare elements, and in C4 we discarded the compounds that are unstable in contact with water. Details of how we implemented C3 and C4 are available in the Supplementary Material (SM). In C5, we selected candidates with appropriate lattices, meaning candidates with at least two perpendicular lattice vectors in the conventional cell. In the final step (C6), we calculated the lattice mismatch between selected perovskite substrates and the coating

materials that survived from C5. This last step produced some coating materials with several phases. In such cases, we prioritized the phase with the least lattice mismatch to MAPbI<sub>3</sub>. The other crystal phases are presented in the SM.

As substrates, we chose 12 ABX<sub>3</sub> perovskites (A = Cs/MA, B = Sn/Pb, and X = Cl/Br/I) that are commonly used in halide-perovskite-based devices. We optimized the structure of the tetragonal P4/mbm phase of CsBX<sub>3</sub> and the tetragonal (quasi) I4/mcm phase of MABX<sub>3</sub> using PBE<sup>30</sup> (to stay consistent with AFLOW data<sup>34</sup>) and the analytic stress tensor<sup>35</sup> implemented in the all-electron numeric-atom-centered orbital code FHI-AIMS<sup>36-38</sup>. Details of the DFT calculations are given in the SM. Upon a test calculation, we selected the (001) crystal planes of the perovskites (Figs. 2a and b) since they are the most stable surface of these materials. We determined the lattice mismatch based on the lattice constants alone and did not carry out any interface calculations with DFT. Figure 2c shows the two “virtual surface models” considered in this work. We did not consider larger surface models, since they would make further computational modeling intractable.

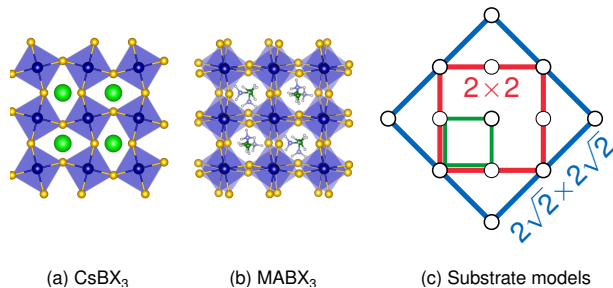


FIG. 2. (001) plane of tetragonal CsBX<sub>3</sub> (a) and MABX<sub>3</sub> (b). The red square in (c) depicts the  $2 \times 2$  and the blue the  $2\sqrt{2} \times 2\sqrt{2}$  unit cell in the (001) plane of of ABX<sub>3</sub>. The green square denotes the square primitive cell. Empty circles indicate the lattice points (e.g., B-sites) at the (001) plane.

From the PBE-optimized lattice constants, we calculated the lattice mismatch at each coating-perovskite interface. To avoid large strain, we required that the coatings should have rectangular lattice planes with small miller indices, e.g., the (100) plane of the cubic lattice or the (11 $\bar{2}$ 0) plane of the hexagonal lattice. More details of this selection is given in the SM. If the lattice constant of the coating and the perovskite are  $a_c$  and  $a_p$  along one direction, then the lattice mismatch is,

$$\gamma \triangleq \frac{ma_c - a_p}{ma_c} \times 100\%, \quad m \in \mathbb{N}. \quad (1)$$

$m$  is the integer that minimizes  $|\gamma|$ . We set the criterion  $\gamma \in (-5, +5)\%$  as shown in Fig. 1.

With the high-throughput screening scheme in Fig. 1, we extracted 93 inorganic semiconductor coating candidates (39 binaries and 54 ternaries) from AFLOW. In addition, there are  $\sim 1000$  suitable ternary compounds, for which we could not find any data on their solubility in water. These remaining compounds will be investigated further in the future.

Figure 3 shows the calculated lattice mismatch between the candidates and the 12 ABX<sub>3</sub> perovskite substrates. Panels 3a and b reveal that several materials with cubic or tetragonal lattices can be used to coat most of the investigated perovskites: ZnS, BN, some fluorides (BiF<sub>3</sub>, MoF<sub>3</sub> and AgSbF<sub>6</sub>), some binary oxides (Bi<sub>2</sub>O<sub>3</sub> in both cubic and tetragonal phases, Ce<sub>2</sub>O<sub>3</sub>, BeO, PbO, TiO<sub>2</sub>-anatase, NiO and tetragonal SiO<sub>2</sub>) and a large range of ternary oxides. In contrast, Figures. 3c and d show that most of the materials that are in neither the cubic nor the tetragonal phase can only cover a small range of perovskite substrates. This is because the  $|\gamma| < 5\%$  criterion must be satisfied by two lattice constants, which makes the coating less “versatile” in these phases.

From Figs. 3a and b, one can immediately deduce that the lattice mismatch increases from  $-5$  to  $5\%$  as the lattice constant of the substrates increases. The yellow spots show the most promising candidates with mismatch  $< 1\%$ . Only a few coating candidates with “non-square” planes survived our screening criteria. This is because in such materials, at least two lattice constants must have lattice mismatch within  $-5$  and  $5\%$ . For instance, the  $\gamma$  values for the interface between the hexagonal phase of Bi<sub>2</sub>O<sub>3</sub> at MAPbBr<sub>3</sub> interface are  $-6.5\%$  and  $0.73\%$  along the  $a$ - and  $c$ -axis, respectively. Thus Bi<sub>2</sub>O<sub>3</sub> would not be a suitable candidate to coat MAPbBr<sub>3</sub>.

As a first consistency check, we compared the material candidates in Figs. 3a and b to materials that have already been used as transport or mesoporous scaffold layers in PSCs. We found that our search is consistent with common materials such as: NiO as HTM in PSCs<sup>39</sup>, as well as ZnO<sup>39</sup> and TiO<sub>2</sub><sup>40</sup> as electron-transporting materials (ETMs). Similarly, our candidate materials included ZrO<sub>2</sub><sup>41</sup> and Al<sub>2</sub>O<sub>3</sub><sup>42</sup> which are used as mesoporous scaffolds in PSCs.

Aside from the commonly known metal oxides used in PSCs, we discovered some surprising binary candidates (MoF<sub>3</sub>, GaN, BiF<sub>3</sub>, Si<sub>3</sub>N<sub>4</sub> and BN) that have properties suitable to coat the photovoltaic-active halide perovskites (Fig. 3a). Similarly, for ternaries we found BaAl<sub>2</sub>S<sub>4</sub>, AgSbF<sub>6</sub>, BaSiF<sub>6</sub> and BaGeF<sub>6</sub>. These materials came as surprise since they are usually not considered in PSCs due to their high melting temperatures. However, with new coating techniques such as radio-frequency sputtering<sup>43</sup>, pulsed laser deposition<sup>44</sup>, vapor-deposition<sup>45</sup> and modified hybrid methods such as spin-coating/vapor-deposition<sup>46</sup>, these materials become contenders as effective coating materials for future PSC devices.

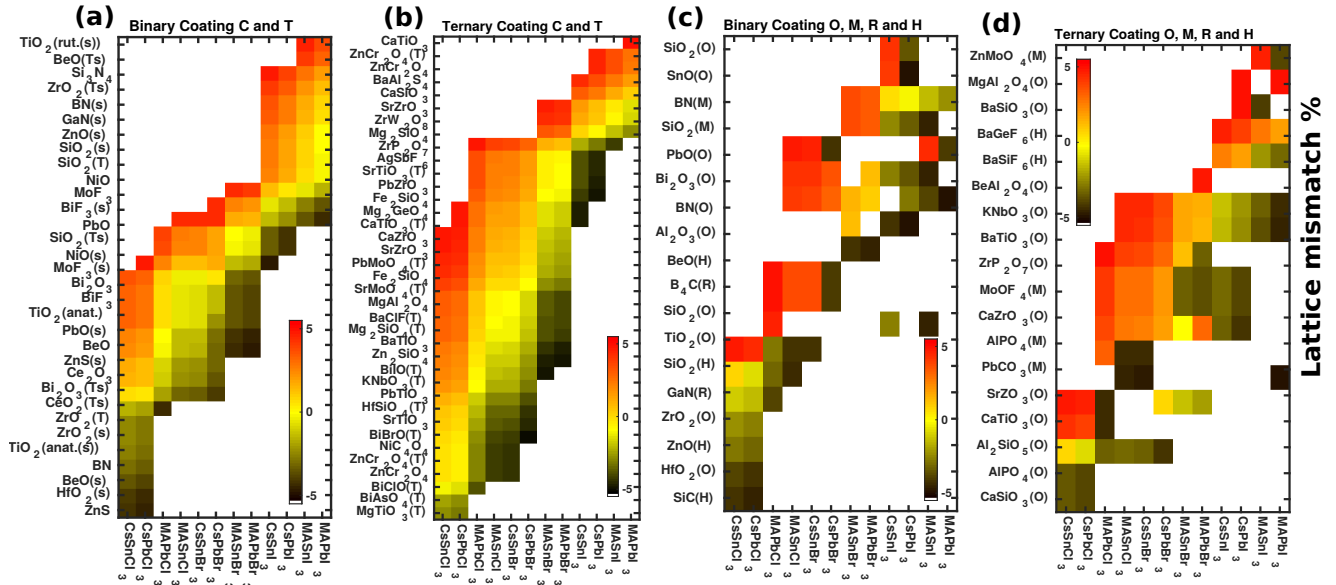


FIG. 3. Calculated lattice mismatch ( $\gamma$ ) between the considered perovskites (horizontal axes) and suitable coating materials (vertical axes). C, T, O, M, H and R are short for cubic, tetragonal, orthorhombic, monoclinic, hexagonal and rhombohedral crystal structures, respectively. s denotes  $2\sqrt{2} \times 2\sqrt{2}$  perovskite substrates, all others are  $2 \times 2$ . Panel shows (a) binary C (unlabeled) and T coatings, (b) ternary C and T coatings, (c) and (d) “non-square” (i.e., O, M, H and R) for binary and ternary coatings.

Of particular interest are the potential coating materials for  $\text{MAPbI}_3$ , the most common photoabsorber in PSCs. Interestingly, our screening procedure reveals that  $\text{Al}_2\text{O}_3$  (Fig. 3c), which is the most common mesoporous material in today’s PSC architectures<sup>5</sup>, does not have the minimum lattice mismatch for coating  $\text{MAPbI}_3$ .  $\text{ZnO}$ ,  $\text{NiO}$ ,  $\text{CaSiO}_3$ ,  $\text{SiO}_2$ ,  $\text{SrZrO}_3$ ,  $\text{BaAl}_2\text{S}_4$ ,  $\text{GaN}$ ,  $\text{MoF}_3$ ,  $\text{BN}$ ,  $\text{Si}_3\text{N}_4$  and  $\text{ZrO}_2$  lead to better lattice match. The actual strain values for  $\text{MAPbI}_3$  can be found in the far right column of each panel in Fig. 3

Next we briefly address the charge carrier properties of the potential candidates. Table I lists the PBE band gaps of the found candidate coatings for  $\text{MAPbI}_3$  provided by AFLOW<sup>29</sup>, together with the dominant charge carrier type (n- or p-type). Here, we observe that intrinsic p-type semiconductors such as  $\text{NiO}$  and  $\text{PbO}$ , will not only protect PSCs against ambient conditions, but could also serve as efficient HTMs to replace the inefficient *Spiro*-OMeTAD.

We also found insulators such as  $\text{ZrO}_2$ ,  $\text{Si}_3\text{N}_4$ , and  $\text{BeO}$  (Table I). Due to the large band gap of these materials and their insolubility in water, they can be used as efficient mesoporous scaffolds to passivate PSCs against degradation. Additionally,  $\text{BN}$  could be used as a p- or n-type semiconductor with different doping mechanisms (Table I). It was recently reported that  $\text{BiF}_3$  has a high-lying valence band<sup>47,48</sup> thus potentially being a good HTM. Also  $\text{HfO}_2$  could be engineered into a p-type material by controlling the oxygen vacancy content<sup>49</sup>.

Lastly, we briefly comment on realistic coating interfaces.

The actual phase of the coating material and the structure of the interface depend on many factors such as the perovskite surface structure and properties, the deposition method, the deposition conditions, as well as the coating thickness. These factors are not included in our database study. An atomistic description of coating-perovskite interfaces requires further computational (e.g., DFT) and experimental work. Results from such future work, such as the stability of the coating materials, could then be incorporated as additional criteria in our screening procedure.

In summary, we have developed a systematic and efficient screening scheme for perovskite coating materials. Our scheme reduces the  $\sim 1.8$  million materials entries in AFLOW to 93 possible coating candidates for a series of perovskite photoabsorbers in PSCs. We have identified inexpensive HTMs ( $\text{NiO}$  and  $\text{PbO}$ ) that can replace the inefficient and expensive *Spiro*-OMeTAD, as well as several efficient ETMs (e.g.,  $\text{ZnO}$ ) for PSCs. Our results feature new materials beyond metal oxides that will not only enhance the stability of PSCs but also serve as a starting point in the search of novel device materials for emergent PSC technologies.

We gratefully thank M. Todorović and G.-X. Zhang for insightful discussions. We acknowledge the computing resources by the CSC-IT Center for Science and the Aalto Science-IT project. An award of computer time was provided by the Innovative and Novel Computational Impact on Theory and Experiment (INCITE) program. This research used resources of the Argonne Lead-

TABLE I. Selected candidate coating materials for MAPbI<sub>3</sub>. Listed are their band gaps (in eV, data from AFLOW<sup>29</sup>), space groups, and dominant charge carriers (n- or p-type conductivity) with corresponding references. Intrinsic n- and p-type materials, and n- and p-type dopable materials, are labeled by N, P, n and p, respectively.

Coating	Space group	Gap	Cond.	Refs.	Coating	Space group	Gap	Cond.	Refs.
CaSiO <sub>3</sub>	P43m	3.67			PbO	P4/nmm	1.66	P	50
BaAl <sub>2</sub> S <sub>4</sub>	Pa3̄	3.65			ZnO	F43m	1.69	N	51
SiO <sub>2</sub>	Fm3̄m	1.73			CaZrO <sub>3</sub>	Pm3̄m	3.21		
MoF <sub>3</sub>	Pm3̄m	1.74			GaN	F43m	1.75		
NiO	Fm3̄m	1.79	P	51	ZrO <sub>2</sub>	P4 <sub>2</sub> /nmc	3.86		
BiF <sub>3</sub>	Fm3̄m	3.95		48	HfO <sub>2</sub>	P4 <sub>2</sub> /nmc	4.01	p	49
BaTiO <sub>3</sub>	Pm3̄m	2.13			BN	F43m	4.46	n,p	
BN	P6 <sub>3</sub> mc	5.21	n,p		PbZrO <sub>3</sub>	Pm3̄m	2.28		
HfSiO <sub>4</sub>	I4 <sub>1</sub> /amd	5.31			CaTiO <sub>3</sub>	Pm3̄m	2.36		
BeO	Fm3̄m	8.18			Si <sub>3</sub> N <sub>4</sub>	Fm3̄m	3.33		

ership Computing Facility, which is a DOE Office of Science User Facility supported under Contract DE-AC02-06CH11357. This project has received funding from the European Union's Horizon 2020 research and innovation programme under grant agreement No 676580 with The

Novel Materials Discovery (NOMAD) Laboratory, European Center of Excellence, the Väisälä Foundation, as well as the Academy of Finland through its Centres of Excellence Programme (2015-2017) under project number 284621 and its Key Project Funding scheme under project number 305632.

- <sup>1</sup> H. J. Snaith, *J. Phys. Chem. Lett.* **4**, 3623 (2013).
- <sup>2</sup> M. A. Green, A. Ho-Baille, and H. J. Snaith, *Nat. Photon.* **8**, 506 (2014).
- <sup>3</sup> M. Saliba, *Science* **359**, 388 (2018).
- <sup>4</sup> H.-S. Kim, C.-R. Lee, J.-H. Im, K.-B. Lee, T. Moehl, A. Marchioro, S.-J. Moon, R. Humphry-Baker, J.-H. Yum, J. E. Moser, et al., *Sci. Rep.* **2**, 591 (2012).
- <sup>5</sup> M. M. Lee, J. Teuscher, T. Miyasaka, T. N. Murakami, and H. Snaith, *Science* **338**, 643 (2012).
- <sup>6</sup> S. D. Stranks, G. E. Eperon, G. Grancini, C. Menelaou, M. J. P. Alcocer, T. Leijtens, L. M. Herz, A. Petrozza, and H. J. Snaith, *Science* **342**, 341 (2013).
- <sup>7</sup> G. Xing, N. Mathews, S. Sun, S. S. Lim, Y. M. Lam, M. Grätzel, S. Mhaisalkar, and T. C. Sum, *Science* **342**, 344 (2013).
- <sup>8</sup> G. E. Eperon, G. M. Paternò, R. J. Sutton, A. Zampetti, A. A. Haghighirad, F. Cacialli, and H. J. Snaith, *J. Mater. Chem. A* **3**, 19688 (2015).
- <sup>9</sup> J. Troughton, K. Hooper, and T. M. Watson, *Nano Energy* **39**, 60 (2017).
- <sup>10</sup> G. Niu, W. Li, F. Meng, L. Wang, H. Dong, and Y. Qiu, *J. Mater. Chem. A* **2**, 705 (2014).
- <sup>11</sup> G. Niu, X. Guo, and L. Wang, *J. Mater. Chem. A* **3**, 8970 (2015).
- <sup>12</sup> J. Huang, S. Tan, P. D. Lund, and H. Zhou, *Energy Environ. Sci.* **10**, 2284 (2017).
- <sup>13</sup> I. Mesquita, L. Andrade, and A. Mendes, *Renew. Sustain. Energy Rev.* **82**, 2471 (2018).
- <sup>14</sup> A. Ciccioli and A. Latini, *J. Phys. Chem. Lett.* **9**, 3756 (2018).
- <sup>15</sup> G.-H. Kim, H. Jang, Y. J. Yoon, J. Jeong, S. Y. Park, B. Walker, I.-Y. Jeon, Y. Jo, H. Yoon, M. Kim, et al., *Nano Lett.* **17**, 6385 (2017).
- <sup>16</sup> F. Li, J. Yuan, X. Ling, Y. Zhang, Y. Yang, S. H. Cheung, C. H. Y. Ho, X. Gao, and W. Ma, *Adv. Funct. Mater.* **18**, 1706377 (2018).
- <sup>17</sup> F. Matteocci, L. Cinà, E. Lamanna, S. Cacovich, G. Divitini, P. A. Midgley, C. Ducati, and A. di Carlo, *Nano Energy* **30**, 162 (2016).
- <sup>18</sup> R. Cheacharoen, N. Rolston, D. Harwood, K. A. Bush, R. H. Dauskardt, and M. D. McGehee, *Energy Environ. Sci.* **11**, 144 (2018).
- <sup>19</sup> R. Cheacharoen, C. C. Boyd, G. F. Burkhard, T. Leijtens, J. A. Raiford, K. A. Bush, S. F. Bent, and M. D. McGehee, *Sustain. Energy Fuels* **2**, 2398 (2018).
- <sup>20</sup> L. N. Quan, M. Yuan, R. Comin, O. Voznyy, E. M. Beaugregard, S. Hoogland, A. Buin, A. R. Kirmani, K. Zhao, A. Amassian, et al., *J. Am. Chem. Soc.* **138**, 2649 (2016).
- <sup>21</sup> L. Dou, *J. Mater. Chem. C* **5**, 11165 (2017).
- <sup>22</sup> C. Ran, J. Xi, W. Gao, F. Yuan, T. Lei, B. Jiao, X. Hou, and Z. Wu, *ACS Energy Lett.* **3**, 713 (2018).
- <sup>23</sup> Z. Wang, A. M. Ganose, C. Niu, and D. O. Scanlon, *J. Mater. Chem. A* **6**, 5652 (2018).
- <sup>24</sup> J. H. Noh, S. H. Im, J. H. Heo, T. N. Mandal, and S. I. Seok, *Nano Lett.* **13**, 1764 (2013).
- <sup>25</sup> C. Yi, J. Luo, S. Meloni, A. Boziki, N. Ashari-Astani, C. Grätzel, S. M. Zakeeruddin, U. Röhrlisberger, and M. Grätzel, *Energy Environ. Sci.* **9**, 656 (2016).
- <sup>26</sup> Y. Zhou, Z. Zhou, M. Chen, Y. Zong, J. Huang, S. Pang, and N. P. Padture, *J. Mater. Chem. A* **4**, 17623 (2016).
- <sup>27</sup> H. Tan, A. Jain, O. Voznyy, X. Lan, F. P. G. de Arquer, J. Z. Fan, R. Quintero-Bermudez, M. Yuan, B. Zhang, Y. Zhao, et al., *Science* **355**, 722 (2017).
- <sup>28</sup> M. Saliba, S. Orlandi, T. Matsui, S. Aghazada, M. Cavazz-

- ini, J.-P. Correa-Baena, P. Gao, R. Scopelliti, E. Mosconi, K.-H. Dahmen, et al., *Nat. Energy* **1**, 15017 (2016).
- <sup>29</sup> S. Curtarolo, W. Setyawan, G. L. W. Hart, M. Jahnatek, R. V. Chepulskii, R. H. Taylor, S. Wang, J. Xue, K. Yang, O. Levy, et al., *Comput. Mater. Sci.* **58**, 218 (2012).
- <sup>30</sup> J. P. Perdew, K. Burke, and N. Ernzerhof, *Phys. Rev. Lett.* **77**, 3865 (1996).
- <sup>31</sup> L. J. Sham and M. Schlüter, *Phys. Rev. Lett.* **51**, 1888 (1983).
- <sup>32</sup> J.-H. Ryou, R. Kanjolia, and R. D. Dupuis, in *Chemical Vapour Deposition: Precursors, Processes and Applications*, edited by A. C. Jones and M. L. Hitchman (RSC Publishing, Cambridge, UK, 2009), p. 272.
- <sup>33</sup> M. Y. Yeh, Y.-J. Liao, D. S. Wu, C.-L. Huang, and C.-D. Yang, in *Advanced Materials: Physics, Mechanics and Applications*, edited by S.-H. Chang, I. A. Parinov, and V. Y. Topolov (Springer, London, UK, 2014), p. 45.
- <sup>34</sup> R. H. Taylor, F. Rose, C. Toher, O. Levy, K. Yang, M. Buongiorno Nardelli, and S. Curtarolo, *Comput. Mater. Sci.* **93**, 178 (2014).
- <sup>35</sup> F. Knuth, C. Carbogno, V. Atalla, V. Blum, and M. Scheffler, *Comput. Phys. Commun.* **190**, 33 (2015).
- <sup>36</sup> V. Blum, R. Gehrke, F. Hanke, P. Havu, V. Havu, X. Ren, K. Reuter, and M. Scheffler, *Comput. Phys. Commun.* **180**, 2175 (2009).
- <sup>37</sup> V. Havu, V. Blum, P. Havu, and M. Scheffler, *JCoP* **228**, 8367 (2009).
- <sup>38</sup> S. V. Levchenko, X. Ren, J. Wierferink, R. Johanni, P. Rinke, V. Blum, and M. Scheffler, *Comput. Phys. Commun.* **192**, 60 (2015).
- <sup>39</sup> W.-C. Lai, K.-W. Lin, T.-F. Guo, P. Chen, and Y.-Y. Liao, *AIP Adv.* **8**, 015109 (2018).
- <sup>40</sup> Q. Chen, H. Zhou, Z. Hong, S. Luo, H.-S. Duan, H.-H. Wang, Y. Liu, G. Li, and Y. Yang, *J. Am. Chem. Soc.* **136**, 622 (2014).
- <sup>41</sup> M. A. Mejía Escobar, S. Pathak, J. Liu, H. J. Snaith, and F. Jaramillo, *ACS Appl. Mater. Interfaces* **9**, 2342 (2017).
- <sup>42</sup> H. Si, Q. Liao, Z. Zhang, Y. Li, X. Yang, G. Zhang, Z. Kang, and Y. ZHANG, *Nano Energy* **22**, 223 (2016).
- <sup>43</sup> J. M. C. da Silva Filho, V. A. Ermakov, and F. C. Marques, *Sci. Rep.* **8**, 1563 (2018).
- <sup>44</sup> Y. Liang, Y. Yao, X. Zhang, W.-L. Hsu, Y. Gong, J. Shin, E. D. Wachsman, M. Dagenais, and I. Takeuchi, *AIP Adv.* **6**, 015001 (2016).
- <sup>45</sup> J. Ávila, C. Momblona, P. P. Boix, M. Sessolo, and H. J. Bolink, *Joule* **1**, 431 (2017).
- <sup>46</sup> H. Dong, Z. Wu, B. Xia, J. Xi, F. Yuan, S. Ning, L. Xiao, and X. Hou, *Chem. Commun.* **51**, 8986 (2015).
- <sup>47</sup> C. Feng, F. Teng, Z. Liu, C. Chang, Y. Zhao, S. Wang, M. Chen, W. Yao, and Y. Zhu, *J. Mol. Catal. A: Chem.* **401**, 35 (2015).
- <sup>48</sup> R. T. Poole, J. Liesegang, R. C. G. Leckie, J. G. Jenkin, and J. B. Peel, *Phys. Rev. B* **13**, 896 (1976).
- <sup>49</sup> E. Hildebrandt, J. Kurian, M. M. Müller, T. Schroeder, H.-J. Kleebe, and L. Alff, *Appl. Phys. Lett.* **99**, 112902 (2014).
- <sup>50</sup> L. M. Droessler, Ph.D. thesis, University of Oxford (2014).
- <sup>51</sup> V. Stevanović, S. Lany, D. S. Ginley, W. Tumas, and A. Zunger, *Phys. Chem. Chem. Phys.* **16**, 3706 (2014).

**Supplementary Material for  
Database-driven high-throughput study for hybrid perovskite coating materials**

Azimatu Seidu,<sup>1</sup> Lauri Himanen,<sup>1</sup> Jingrui Li,<sup>1</sup> and Patrick Rinke<sup>1</sup>

<sup>1</sup>*Department of Applied Physics, Aalto University, P.O.Box 11100, FI-00076 AALTO, Finland*

**S1. DETAIL OF C3 AND C4 IN THE DATA SCREENING SCHEME**

In C3, we excluded compounds that contain:

- radioactive elements,
- toxic elements (Cd, Hg, Tl),
- noble metals as well as Re, Au and Te due to their very low abundance in earth's crust.

We also discarded all compounds containing H due to their high possibility of hydrolysis. In this work we only consider Ce to represent the whole rare-earth (lanthanides, scandium and yttrium) family as it is the most abundant member.

With the help of the CRC handbook for physics and chemistry<sup>?</sup> and other resources, we generated the data in C4 by manually discarding all compounds that are unstable in water, i.e., water soluble, reacting with water, or decomposing in water. However, the CRC handbook did not have solubility data on all our selected structures, leaving a huge set of data ( $\sim 4000$ ) mainly from the ternary class of compounds. We therefore need a more reliable reference to classify such compounds. In addition, compounds that have a very low melting point, are explosive, or easy to release poisonous gases were not included.

**S2. DENSITY-FUNCTIONAL-THEORY CALCULATIONS OF HALIDE PEROVSKITES**

DFT calculations were performed with the all-electron numeric-atom-centered orbital code FHI-AIMS<sup>?</sup> <sup>?</sup> <sup>?</sup>. For all calculations, we used *tight* basis set and stress-tensor<sup>?</sup> implemented in FHI-AIMS. Scalar relativistic effect by means of the zero-order regular approximations (ZORA)<sup>?</sup> were included. The computational details were slightly different for the two perovskite classes considered in this work. We used the tetragonal  $P_4/mbm$  phase to construct  $2 \times 2 \times 2$  supercell models for  $CsBX_3$ , and relaxed the structures with a  $\Gamma$ -centered  $4 \times 4 \times 4$   $k$ -point mesh. While for  $MABX_3$ , we used the tetragonal (quasi)  $I_4/mcm$  phase and optimized  $\sqrt{2} \times \sqrt{2} \times 2$  supercells with a  $6 \times 4 \times 4$   $k$ -point mesh. From the optimized tetragonal structures (with lattice constants  $a, b = a, c$ ), we chose the (001) planes to construct our virtual surface models for the lattice-mismatch calculations. The corresponding lattice constants are listed in Table S1.

TABLE S1. PBE-optimized lattice constants (in Å) of (001) surfaces of the investigated perovskites: single cells ( $a_0$ ),  $2 \times 2$  surface cells ( $a_{2 \times 2} = 2a_0$ ) and  $2\sqrt{2} \times 2\sqrt{2}$  surface cells ( $a_{2\sqrt{2} \times 2\sqrt{2}} = 2\sqrt{2}a_0$ ).

Cs-	$a_0$	$a_{2 \times 2}$	$a_{2\sqrt{2} \times 2\sqrt{2}}$	MA-	$a_0$	$a_{2 \times 2}$	$a_{2\sqrt{2} \times 2\sqrt{2}}$
-SnCl <sub>3</sub>	5.60	11.21	15.85	-SnCl <sub>3</sub>	5.76	11.52	16.29
-PbCl <sub>3</sub>	5.62	11.24	15.90	-PbCl <sub>3</sub>	5.82	11.64	16.46
-SnBr <sub>3</sub>	5.83	11.66	16.49	-SnBr <sub>3</sub>	5.99	11.98	16.95
-PbBr <sub>3</sub>	5.87	11.75	16.61	-PbBr <sub>3</sub>	6.01	12.01	17.00
-SnI <sub>3</sub>	6.18	12.37	17.49	-SnI <sub>3</sub>	6.30	12.61	17.83
-PbI <sub>3</sub>	6.23	12.46	17.63	-PbI <sub>3</sub>	6.36	12.72	17.99

### S3. SUGGESTED COATING PATTERNS FOR COATINGS OF DIFFERENT LATTICE SYSTEMS

We only considered rectangular surfaces of coating materials therewith excluding the triclinic phases. Table S2 lists the lattice constants considered in the coating design (i.e., lattice-mismatch calculations). For hexagonal lattices (including trigonal lattices represented in hexagonal), we considered both  $(10\bar{1}0)$  and  $(11\bar{2}0)$  planes.

TABLE S2. Lattice constants of cubic (C), tetragonal (T), orthorhombic (O), hexagonal (H), and monoclinic (M) coating materials considered in lattice-mismatch calculations.

Lattice constants	Considered lattice constants
C $a_c$	$a_c$
T $a_c = b_c, c_c$	$a_c$
O $a_c, b_c, c_c$	$(a_c, b_c), (a_c, c_c)$ or $(b_c, c_c)$
H $a_c = b_c, c_c$	$(a_c, c_c), (\sqrt{3}a_c, c_c)$ $(a_c, \sqrt{3}a_c)$ or $(\sqrt{3}a_c, \sqrt{3}c_c)$
M $a_c, b_c, c_c, \beta \neq 90^\circ$	$(a_c, b_c)$ or $(b_c, c_c)$

### S4. COATING PARAMETERS FOR MAPbI<sub>3</sub>

We have listed the most suitable coating materials for MAPI<sub>3</sub> with their lattice constants, lattice mismatch and their appropriate perovskite substrates in Tab. S3. Here, we only listed the candidates with lattice mismatch  $< 2\%$ . Binary and ternary coating materials with square planes are listed in (Tab. S3a and (Tab. S3b). We have also listed the lattice mismatch (along 2-axis) at the coating-MAPI<sub>3</sub> interface for binary and ternary coatings with “non-square” planes (Tab. S3c and d).

### S5. COATING MATERIALS WITH MULTIPLE PHASES

Suitable coating materials for PSCs with multiple phases are shown in S1. Here, we show all the remaining coating candidates that were not shown in the main text. We also show the possible coating candidates for both  $2 \times 2$  and  $2\sqrt{2} \times 2\sqrt{2}$  perovskite substrates used in this work. Here, we use “s” to denote coating materials for the  $2\sqrt{2} \times 2\sqrt{2}$  surfaces. Cubic phases are not labelled, “T”, “O”, “R” and “H” denote tetragonal, monoclinic, rhombohedral and hexagonal structures respectively. We used the numbers, 1, 2, 3, ... to differentiate between coating materials of the same structures but different phases.

TABLE S3. Most suitable coating for MAPbI<sub>3</sub> with  $|\gamma| < 5\%$ : (a) C and T binary coatings, (b) C and T ternary coatings, and (c) H, O and M coatings. Shown are the lattice constants  $a_c$  (in Å) of each coating considered in the  $\gamma$  calculations, the lattice mismatch  $\gamma$  (in %) and the integer  $m$  defined in Eqs. (1) and (2) of the main text, and the size ( $2 \times 2$  and  $2\sqrt{2} \times 2\sqrt{2}$ , denoted by I and II, respectively) of perovskite (P) substrate.

(a) C/T binary coatings / MAPbI <sub>3</sub>											
	Structure	$a_c$	$\gamma$	$m$	P		Structure	$a_c$	$\gamma$	$m$	P
MoF <sub>3</sub>	Pm $\bar{3}$ m	4.17	-1.58	4	I	NiO	Fm $\bar{3}$ m	4.23	-0.33	3	I
SiO <sub>2</sub>	I $\bar{4}$ 3m	8.98	-0.144	1	I	ZnO	F $\bar{4}$ 3m	4.50	-0.01	3	II
GaN	F $\bar{4}$ 3m	4.53	0.65	3	II	BN	F $\bar{4}$ 3m	3.62	0.73	4	II
ZrO <sub>2</sub>	P4 <sub>2</sub> /nmc	3.59	1.30	3	II	Si <sub>3</sub> N <sub>4</sub>	I <sub>43</sub> d	6.49	1.93	3	II
ZnO	Fm $\bar{3}$ m	4.21	-0.75	4	II	BeO	Fm $\bar{3}$ m	3.65	1.39	3	I
SiO <sub>2</sub>	F $\bar{3}$ m	4.58	1.88	3	I	BN	P4 <sub>2</sub> /mmc	9.13	1.46	1	I

(b) C/T ternary coatings / MAPbI <sub>3</sub>											
	Structure	$a_c$	$\gamma$	$m$	P		Structure	$a_c$	$\gamma$	$m$	P
PbZrO <sub>3</sub>	Pm $\bar{3}$ m	4.21	-0.75	4	II	CaZrO <sub>3</sub>	Pm $\bar{3}$ m	4.16	-1.89	4	II
ZrW <sub>2</sub> O <sub>8</sub>	P2 <sub>1</sub> 3	3.54	-1.66	1	I	SrZrO <sub>3</sub>	P2 <sub>1</sub> 3	3.55	-1.41	5	I
CaSiO <sub>3</sub>	Pm $\bar{3}$ m	3.61	0.27	4	I	BaAl <sub>2</sub> S <sub>4</sub>	Pa $\bar{3}$	3.65	1.40	3	I
SrZrO <sub>3</sub>	P4/mbm	3.17	-0.42	4	II	PbTiO <sub>3</sub>	I4/m	12.71	-0.10	1	II

(c) H/O/M/R binary coatings / MAPbI <sub>3</sub>											
	Structure	$a_c$	$\gamma$	$m$	P		Structure	$a_c$	$\gamma$	$m$	P
BN	R3m	2.51	-1.27	5	I	BN	P6 <sub>3</sub> mc	2.56	0.42	5	I
		12.16	* - 4.59	1	I			4.23	-0.36	3	I
SiO <sub>2</sub>	P6 <sub>5</sub> 22	7.36	0.20	$\sqrt{3}$	I	SiO <sub>2</sub>	Cmca	9.09	1.01	2	I
		7.06	* - 4.07	$\sqrt{3}$	I			9.36	3.90	2	II
SiC	P3m1	3.09	-2.79	4	I						
		12.66	-0.52	1	I						

(d) H/O/M/R ternary coatings / MAPbI <sub>3</sub>											
	Structure	$a_c$	$\gamma$	$m$	P		Structure	$a_c$	$\gamma$	$m$	P
Al <sub>2</sub> SiO <sub>5</sub>	Cmcm	3.56	-0.96	5	II	BaSiF <sub>6</sub>	R $\bar{3}$ m	7.33	-0.23	$\sqrt{3}$	I
		9.29	1.96	2	II			7.12	* - 3.20	$\sqrt{3}$	I
MgSiO <sub>3</sub>	Pbcn	8.86	-1.59	2	II	MgAl <sub>2</sub> O <sub>4</sub>	Cmcm	2.81	2.99	6	II
		9.36	3.90	2	II			9.27	*4.94	2	II
MgSiO <sub>3</sub>	Pbca	8.86	-0.61	2	II	BaGeF <sub>6</sub>	R $\bar{3}$ m	7.48	1.82	$\sqrt{3}$	I
		18.45	2.46	1	II			7.24	-1.45	$\sqrt{3}$	I

\*:  $=\sqrt{3} \cdot 3.62$



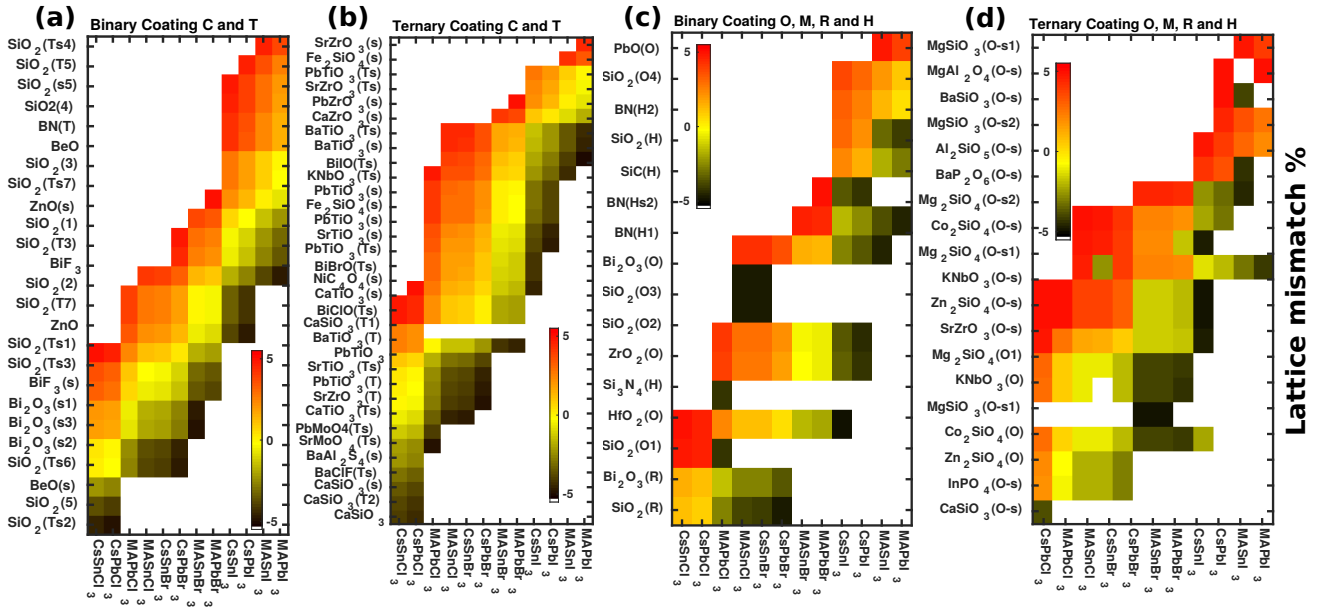


FIG. S1. Calculated lattice mismatch ( $\gamma$ ) between considered perovskites (horizontal axes) and all coating materials (vertical axes) outcome from the screening scheme: C, T, O, M, H and R represent, cubic, tetragonal, orthorhombic, monoclinic, hexagonal and rhombohedral crystal structures, respectively. ‘s’ denotes the  $2\sqrt{2} \times 2\sqrt{2} \times 2\sqrt{2}$  perovskite substrates. (a) binary C (unlabeled) and T coatings, (b) ternary C and T coatings, (c) and (d) “non-square” (i.e., O, M, H and R) for binary and ternary coatings. Numbers 1, 2 ... denote materials of the same crystal structures having different phases